SELECTIVE ELECTROCHEMICAL REDUCTION OF CO_2 TO HIGH VALUE CHEMICALS

Grant agreement no.: 851441
***Start date**: 01.01.2020 – **Duration**: 36 months*
***Project Coordinator**: Dr. Brian Seger - DTU*

DELIVERABLE REPORT

3.1 REPORT ON RECYCLE AND TEMPERATURE EFFECTS ON ELECTROCHEMICAL CO2 REDUCTION (ECO2R)	
Due Date	31/1/2022
Author (s)	Carlos Andres Giron Rodriguez, Qiucheng Xu, Brian Seger
Workpackage	3
Workpackage Leader	Brian Seger
Lead Beneficiary	DTU
Date released by WP leader	18-01-2022
Date released by Coordinator	18-01-2022

DISSEMINATION LEVEL		
PU	*Public*	***X***
PP	*Restricted to other programme participants (including the Commission Services)*	
RE	*Restricted to a group specified by the consortium (including the Commission Services)*	
CO	*Confidential, only for members of the consortium (including the Commission Services)*	

NATURE OF THE DELIVERABLE		
R	*Report*	***X***
P	*Prototype*	
D	*Demonstrator*	
O	*Other*	

SUMMARY	
Keywords	*Electrochemical CO_2 reduction, recycle loop, elevated temperature*
Abstract	This report demonstrates performance variations due to using a recycle loop in CO_2 electrolysis. To allow for the focus to remain on the recycling, an Ag catalyst was used that primarily produced CO. The recycling loop approach showed that it was possible to use this technique to achieve relatively high CO_2 conversions (>70%) while still maintaining high selectivity to CO. As part of this work, we also investigate temperature effects from room temperature to 80 °C. The general trend discovered is that at higher temperatures, selectivity towards H_2 decreases, and the CO selectivity in relation to other CO_2R products increases.
Public abstract for confidential deliverables	

REVISIONS			
Version	**Date**	**Changed by**	**Comments**
0.1	15/1/2022	Qiucheng Xu, Carlos Andres Giron Rodriguez	

REPORT ON RECYCLE AND TEMPERATURE EFFECTS ON ECO2R (ECO2R)

CONTENT

1.1.1 INTRODUCTION

CO_2 flow electrolyzers have been studied extensively in recent years due to their capacity to conduct electrochemical CO_2 reduction (eCO_2R) at high reaction rates with significant selectivity to multi-carbon products [1]. The focus of this field remains to understand the key levers to improve the catalyst properties by facet engineering, nanostructuring, vacancy steering, or manipulating the electrochemical environment (temperature, pressure, or electrolyte) [2–4]. Although the above strategies could promote eCO_2R performance in flow cells, the reported high Faradaic efficiencies at high current densities typically required an excessive amount of CO_2, while single-pass conversions were generally below 10% or even not reported [5-7].

The low CO_2 conversion in these electrolyzers limits the large-scale implementation due to the high separation costs. Based on the techno-economic analysis conducted by Jouny *et al.*, 23% of the total operational cost corresponds to separating gas mixtures from eCO_2R, assuming 10% CO_2 single-pass conversion; while a system capable of guaranteeing 50% of the single-pass CO_2 conversion could reduce these costs by 78% and thus 6% of total costs [8]. In WP8, we are working in techno-economic and LCA analysis to sharpen these parameters due to the separation costs of the different products.

Strategies for enhancing the CO_2 conversion should consider the influence of the electrocatalyst, operating conditions (e.g., feeding rate, current density, applied potentials, reaction temperatures, and operating pressures), and the cell configuration to predict the interplay among them and the conversion to target products [9]. Previous studies focusing on understanding the effect of these parameters in CO_2 single-pass conversion showed that the electrochemical CO_2-single pass conversion could not exceed 43%, independent of the flow rate and current density [10]. However, the total CO_2 consumption could reach around 95%, mainly associated with side reactions, including carbonate formation.

Current cell configurations such as the membrane electrode assemblies (MEA) or reactors with a flowing catholyte can enhance the gas transport compared to H-cells [11]. However, recent investigations using flow cells with alkaline electrolytes have shown limited performance due to CO_2 penetration into the catholyte layer, faster electrode flooding, as well as high ohmic losses from the poor conductivity of the liquid electrolyte solutions [12,13]. The MEA cell type using anion-exchange membranes (AEM) can overcome these effects by removing the catholyte layer and reducing the ohmic overpotential in the cell, despite some limitations in liquid-products quantification and CO_2 crossover [2].

There are different strategies to overcome the low CO_2 conversion in present cell devices, such as creating a recycle line after the cell, following the approaches in biodiesel and low-chain-hydrocarbons industrial production. Taking advantage of promoting the selective consumption of the unreacted CO_2 (as well as intermediate products such as CO or acetaldehyde), the eCO_2R approach of using the recycle loop could improve CO_2 conversion to more highly reduced species compared to a single-pass operation.

As part of WP3, a robust CO_2 electrochemical reaction system with a recycle loop was implemented to study the capability, the effects of CO_2 conversion, and the selectivity for target products. The hypothesis behind the implementation is its ability to operate at lower overpotentials, where some of the CO_2 is reduced to ethanol. However, much of it only reduces to the first intermediate, CO, before being desorbed from the catalyst surface, resulting in a product stream that is primarily CO, ethanol, and other products such as ethylene or C_3 products. Then, with a post-reactor condensation unit, we can pull out the ethanol allowing the CO (as well as unreacted CO_2

and other products) to be recycled back to the reactor. The recycle loop thus gives the CO multiple chances to reduce to ethanol while still operating at a low overpotential.

For the recycle loop approach to work most effectively, the ethanol needs to come off as a vapor. While ethanol has a relatively high vapor pressure, increasing the temperature can significantly enhance the ethanol coming off as a vapor. This is essential as the longer ethanol stays in the reactor as a liquid, the more likely it will migrate to the anode, where it can easily reoxidize to CO_2. Thus, operating at high temperatures is essential for this recycling loop approach.

We also investigate the temperature effects on CO_2 electrolysis of Cu-based GDEs in an MEA-based approach in a temperature range between 25 to 80˚C to enhance the selectivity of C_{2+} products and the energy efficiency while suppressing the hydrogen evolution (HER) and the degradation of the GDE. For this investigation, a robust system for controlling and measuring the temperature of all the system components was developed, and we simultaneously set up proper guidelines to perform these electrocatalytic temperature measurements in a consistent and reproducible way.

1.1.2 DELIVERABLE SCOPE AND DESCRIPTION

The scope of this deliverable is primarily to show the influence of a recycle loop on performance as well as how a CO_2 electrolysis device operates at elevated temperatures. Given the recycle loop is the key enabling technology, the primary focus is on describing the recycle loop capabilities with a lesser focus on temperature effects. In addition, the recycle loop experiments were isolated from the temperature effect experiments so that each effect could be analyzed individually. Showing the optimization of the recycling loop with temperature is beyond the scope of this deliverable, as it will involve integrating and optimizing gas diffusion layers and membranes from WP5 and WP6, coupling the modeling from WP7. While this is ongoing, the results of the complete device optimization, including recycling parameters and temperature, will be reported in Deliverable 3.5 when disseminating the overall optimization of the device.

1.2 Experimental methods

1.2.1 MATERIALS

Ag porous membrane with a nominal pore size of 1.2 µm (Sterlitech Inc., purity 99.97%, area 2.25 cm^2) was used as the cathode. The anode was a commercial IrO_2-coated carbon paper electrode (Dioxide Materials). The anion exchange membranes, AEM, were the Sustainion membrane X37-50 RT (Dioxide Materials), or the developed membranes from the US denoted as MPIP membranes (for detailed information, see the deliverable D6.5 from WP6). For the temperature experiments in Section 1.4, Sputtered Cu (thickness of 150 nm) on carbon paper (SG39BB) was used as the cathode.

1.2.2 EC-reactor setup (Cell configuration)

The experiments were conducted on a commercial electrolyzer (Dioxide Materials), using a zero-gap MEA configuration. The assembly loaded a fresh AEM between the electrodes (cathode area 2.25 cm^2 and anode area 4 cm^2) with PTFE gaskets for electrode protection and electrical insulation. The cell bolts are fastened with an estimated torque of 4 Nm to guarantee sufficient compression and avoid leakages into the system.

1.2.3 Electrochemical Tests

The CO_2 gas-feeding rate (AGA, purity 4.5) in the cathode was set using a volumetric flow controller (Red-y from Voegtlin) and further humidified by sparging into a container filled with Millipore water. The anode side was fed with 0.1 M $KHCO_3$ (Sigma-Aldrich, 99.995% trace metal basis) and recirculated continuously using a diaphragm pump (KNF). Another diaphragm pump for gas and liquids (KNF) was also used for the recycle line and control of the reflux ratio (See Figure 1). A potentiostat (Bio-Logic VSP 300 with booster unit) operated in galvanostatic mode with a range of 50-300 mA/cm^2 was the power source. The standard conditions for gas flow in this work are 273 K and 1 bar, with Ag/AgCl as the reference electrode. For high-temperature experiments, a heating oven with a PSU/box interfaced with a Raspberry Pi and Audrinos was used with a PID controller. A 230 heater (GPIO pin) was connected to thermocouples for the temperature measurement, and a homemade Python program developed at DTU controlled the recycle loop and the reaction temperature in the reaction system.

1.2.4 Product distribution analysis and flow measurements

The cathode outlet stream was measured continuously using a volumetric flow meter (MesaLabs, Defender 530+), while the flow from the recycle loop with a different type of flow meter was able to handle higher humidity's (µFlow Bioprocess control). Quantification of the gas products was determined with a PerkinElmer Clarus 590 gas chromatograph equipped with the Molecular Sieve 13x, and HayeSep Q packed column using Ar (10 mL/min) as the carrier gas and with a thermal conductivity detector (TCD). Experiments focused exclusively on understanding the recycling loop effect do not have any liquid product analysis, despite that Ag does produce CO, H_2, and a small amount of formate under the applied operating conditions. Studies performed by Larrazabal et al. [11] reported Faradaic efficiencies for formate around 15%, meaning the conversions presented in this work on the CO_2 conversion of these type of reactors with the actual conversion is most likely underestimated.

For our temperature experiments, liquid products in the cathode (collected by using a water trap after the CO_2-outlet line) and the anode were collected and quantified with a high-performance liquid chromatography (HPLC) instrument. The instrument consists of an Agilent 1260 Infinity unit with refractive index (RID) and diode array (DAD) detectors, equipped with a Bio-Rad Aminex HPX-87H column. The column was heated isothermally, and an aqueous solution of H_2SO_4 (5 mM with a flow of 0.3 mL/min) served as the eluent, measuring each sample for 60 minutes. Data analysis of the liquid products includes the cathode and the anode products (considering the crossover of the different compounds).

1.2.5 Stoichiometric Reactions

The following section considers the electrocatalytic conversion of CO_2 using Ag as a working electrode (WE), which applies to the experiments performed with the recycling loop. Following this scenario, CO and H_2 are the only significant products involving just two-electron transfer reactions. Performing experiments in the galvanostatic are preferred with respect to potentiostatic mode since the total product generation remains constant (see equations (1) and (2), respectively). During eCO_2R, CO_2 and H_2O can be electrochemically converted to CO, while the H_2O reduction to H_2 (HER) is a competing process.

$$CO_2 + H_2O + 2e^- \rightarrow CO + 2OH^- \qquad (E^O = -0.11\,V\ vs.\,RHE) \qquad (1)$$

$$2H_2O + 2e^- \rightarrow H_2 + 2OH^- \qquad (E^O = 0\,V\ vs.\,RHE) \qquad (2)$$

The reaction at the anode consists mainly of OER under alkaline conditions with AEM is described in equation (3).

$$4OH^- \rightarrow O_2 + 2H_2O + 4e^- \qquad (E^O = 1.23\ V\ vs.RHE) \qquad (3)$$

During CO_2 reduction in flow electrolyzers using $KHCO_3^-$ as an electrolyte, CO_2 from the gas chamber could also be consumed by OH^- ions produced at the cathode, according to equations (4) and (5):

$$CO_2 + OH^- \leftrightarrow HCO_3^- \qquad (pKa = 7.8) \qquad (4)$$

$$HCO_3^- + OH^- \leftrightarrow CO_3^{2-} + H_2O \qquad (pKa = 10.3) \qquad (5)$$

Subsequently, CO_3^{2-}, HCO_3^- and OH^- coming from the cathode could crossover to the anode compartment and be oxidized there [14].

Calculations of the total CO_2 conversion and product selectivity will be briefly described in the following sections. For more details, please refer to MS18 of the current project.

1.2.6 Conversion Rate of CO_2

The conversion rate of CO_2 to CO can be estimated from the flow and carbon balance according to equation (6):

$$X_{CO_2} = \frac{\dot{n}_{CO_2,in} - \dot{n}_{CO_2,out}}{\dot{n}_{CO_2,in}} \approx \frac{\dot{n}_{CO,out}}{\dot{n}_{CO_2,in}} \qquad (6)$$

Where $\dot{n}_{CO_2,in}$ is the molar flow of the inlet CO_2, $\dot{n}_{CO_2,out}$ is the outlet flow of the unreacted CO_2, $\dot{n}_{CO,out}$ is the molar flow rate of CO in the gas effluent measured by the flowmeter and GC, and X_{CO_2} is the CO_2 conversion. We need to remark that equation (6) represents an approximation of the CO_2 conversion to CO, excluding the formate production in the cathode and assuming CO and H_2 as main products.

This equation also does not account for CO_2 equilibration to carbonate. As we have shown in [11], [14], and Deliverable 6.5, the production of every molecule of CO, H_2, and formate (i.e. 2 e^- reduced products) correspond to an equivalent amount of CO_2 converted to bicarbonate. As mentioned previously, this carbonate crosses over the membrane to the anode, and thus it cannot be converted to products. To exclude the carbonate formation and crossover, we can modify equation (6) as follows:

$$X_{CO_2}(excluding\ crossover) = \frac{\dot{n}_{CO,out}}{\dot{n}_{CO_2,in} - \dot{n}_{CO,out} - \dot{n}_{H_2,out} - \dot{n}_{Formate,out}} \qquad (7)$$

Since we cannot detect formate, we will set this value to zero, but in reality, this will be greater than zero, and thus we are effectively underestimating our conversion. Results in the following sections are reported excluding the crossover-effects (based on equations 1-5 and the continuous production and consumption of OH^- in eCO_2R and carbonate processes), which could also lead to an underestimation of the CO_2 conversions

1.2.7 General Mass Balance on zero-gap CO2 electrolysis reactor

The scheme of the CO_2 electrolyzer is presented in Figure 1. Two different mass flow controllers were used to control the humidity of the feeding rate, and the cell's outlet flow passed through a condenser before entering the gas chromatography unit. The gas flow rate was measured at different points of the system using volumetric flowmeters (VFM). The term "reflux ratio" in this report is defined as the ratio of the recycled stream to the outlet stream. The pressure in the different chambers in the EC-cell was controlled by manual backpressure regulators (BPR) from Swagelok and coupled with a pressure indicator.

General Volumetric Balance

$Inlet\ flow\ before\ the\ humidifier$: $F_{11} + F_1 = F_3$

$Inlet\ flow\ through\ the\ cathode$: $F_4 + F_5 = F_6$

$Outlet\ flow$: $F_8 = F_9 + F_{12}$

$Global\ balance$: $F_1 + F_2 + F_{11} = F_9 + F_{14}$

$Reflux\ ratio$: $R = \frac{F_6}{F_{12}}$

Pressure Measurement and regulation: F_1=f($P_{i,g}$) F_{13}=f($P_{i,lcathode}$) F_6=f($P_{out,g}$) F_7=set f($P_{out,g}$) F_{18}=f($P_{in,lanolyte}$) F_{19}=f($P_{out,lanolyte}$) F_{20}=set f($P_{out,g}$) F_{21}=Atmospheric Pressure

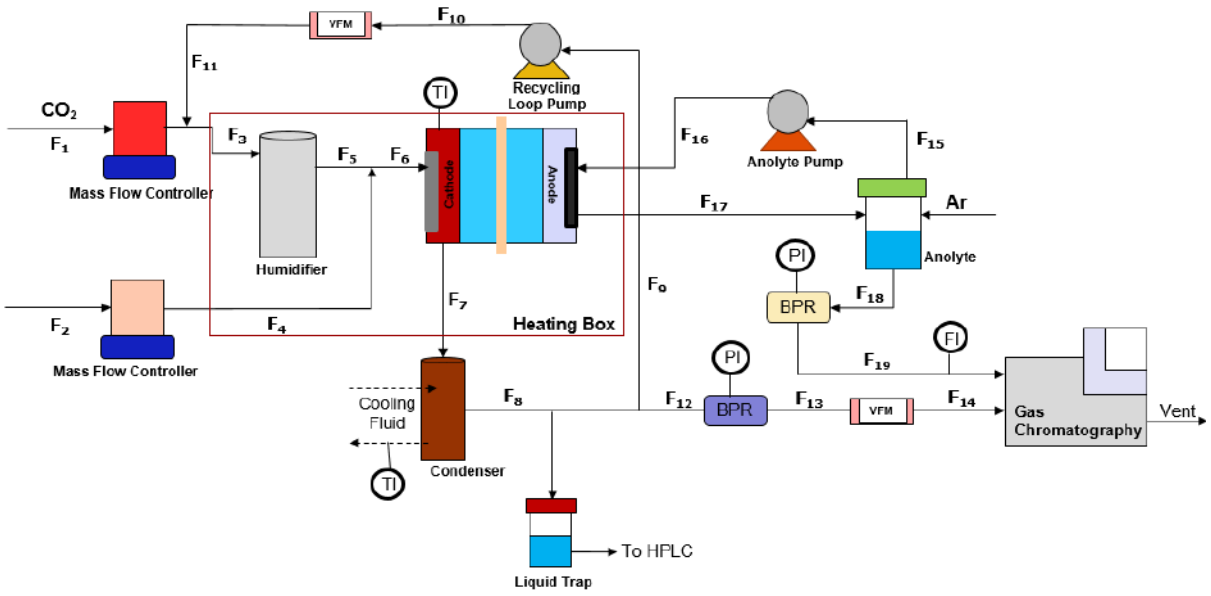

Figure 1: Schematic representation of the CO_2 electrolyzer system

A series of galvanostatic experiments were performed to evaluate the temperature influence on electrocatalytic performance. The obtained results provide insights into how CO_2 diffusion, reaction kinetics, and CO_2 mass transport vary with temperature and affect the overall performance. We observed improvement in reaction rates and a drop in cell voltages at higher temperatures due to the enhancement of membranes' ionic conductivity and water management. The experiments focused on selectivity, and product crossover revealed a specific trend at temperatures above 60˚C for gas and liquid products, setting up the optimal conditions for a stable operation with higher faradaic efficiencies of carbon-based compounds (see Section 1.4).

1.3 Results and Discussion on Recycle Loop

This section focuses on understanding the recycle loop and the temperature effect for CO_2 conversion and selectivity. The CO_2 single-pass, reflux ratio, current density, and CO_2 feeding rate. The temperature for all experiments was set to be 60 °C due to ensure the stability of the commercial AEM.

Although GDE-based electrodes provide commercially relevant conditions, the reported literature conversions are still generally low. In alkaline conditions, the equilibrium between CO_2 and OH^- causes a significant CO_2 consumption. The use of bipolar membranes prevents carbonate formation and the crossover to the anode by selective ion transport. However, it has been reported that the implementation of such types of membranes causes low CO Faradaic efficiency and CO_2 conversions in an MEA type cell [15]. Some previous eCO_2R studies reporting the single-pass CO_2 conversion at different experimental conditions are summarized and compared with this study in Table 1.

Table 1. Single-pass CO_2 conversion reported in the literature for eCO_2R at high current densities

Study	Main Products	jCO_2 (mA/cm^2)	Active Area (cm^2)	CO_2 Flow rate (ml/min)	Duration	Electrolyte pH	% CO_2 conversion	Ref.
Haas et al.	CO	71	10	10,5	Not Reported	7	47,0	[16]
Haas et al.	CO	180	10	100	48 dys.	7	12,5	[16]
Salvatore et al.	CO	105	4	100	12 min	7	3,0	[17]
Salvatore et al.	CO	60	4	100	1 day	7	1,7	[18]
Verma et al.	CO	99	1	17	8 hrs	14,3	4,1	[19]
Verma et al.	CO	200	1	17	4 min	14,3	8,2	[19]
Kutz et al.	CO	190	5	20	40 days	7	33,1	[20]
Hoang et al.	CO	30	1	20	8 hrs	7	7,8	[21]
Li et al.	CO, EtOH, C_2H_4	275	1	7	3 min	14	1,0	[22]
Dinh et al.	C_2H_4	61	1	50	6 days	14,85	0,3	[9]
Dinh et al.	C_2H_4	473	1	50	2.5 min	14,85	2,2	[9]
Ma et al.	EtOH, C_2H_4	138	1	7	3 min	7	22,5	[23]
Jeng and Jiao	CO	80	25	15	Not Reported	7	43	[10]
This study	CO	147	2,25	5	2 hrs	7	37	-

The CO_2 feeding rates were set between 5-50 mL/min at constant current density (200 mA/cm^2) and temperature (60 °C) for the single-pass conversion studies. Figure 2a shows the Faradaic efficiency of gas products at different flow rates, and Figure 2b presents the fraction of CO_2 converted to CO. The compositions of the gaseous products are taken from the last three measurements. One problem regarding the gas diffusion electrodes is their loss of hydrophobicity over time due to the liquid penetration from the catalyst layer to the MPL. This results in electrolyte flooding into the gas diffusion layer, which then prevents the efficient mass transfer of CO_2. Each experiment was operated for 2 hours to avoid these flooding issues, using a fresh Ag-electrode. Based on these results, a proportional relationship between the inlet flow and the CO_2 to CO conversion was discovered, which is similar to the trend reported by Jeng and Jiao in their CO_2-single pass conversions study [10].

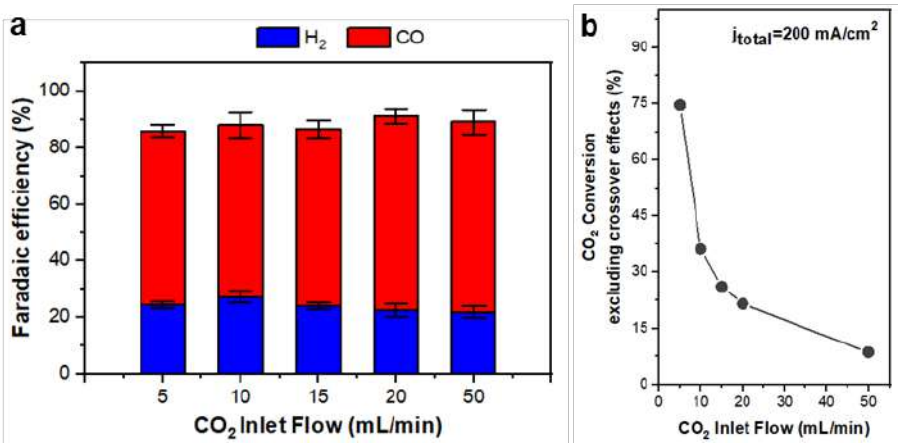

Figure 2: Electrochemical performance of CO_2 reduction at different CO_2 feeding rates at 200 mA/cm^2. **a)** CO Faradaic efficiency and **b)** CO_2 single-pass conversion to CO excluding crossover effects.

By integrating the reactions (1), (2), and (4), this shows that for each CO_2 converted to CO, another CO_2 is consumed by carbonate formation in parallel. This phenomenon happens under the assumption that all produced hydroxyl groups combine with CO_2 to form carbonates, setting a practical, theoretical limit of CO_2 conversion to CO as Jeng and Jiao, using Ag as a catalyst, also described it. The conducted experiments in their work showed a maximal conversion of 37%. However, this value is lower than what it has been reported by that study, which we attribute the differences to mass transfer issues with the cell configuration [10].

In addition, in this report we will alsooperate at elevated temperatures (60-80°C), since this is what must be done industrially due to heat management issues. Noticeably, these results do not vary significantly from those obtained at room temperature (RT), possibly due to shifts of the adsorption equilibria of species at the surface or the CO_2 solubility at low feeding rates [24]. Further experiments at elevated temperatures will be conducted to verify this hypothesis and provide a more in-depth understanding of temperature's contribution to eCO_2R.

1.3.1 Reflux Ratio Study

A recycle line is expected to improve the CO_2 reduction to CO and further overcome the high onset potentials from the first steps of the eCO_2R mechanism. Initially, the outlet flow introduced back to the inlet CO_2 flow is defined by the reflux ratio (RR), a parameter described in Section 4.2.3 and regulated by the measurements of the outlet flows in the system. Ranges between 1-12 were defined for the RR, and each run was conducted with new electrodes and

a new AEM. The inlet CO_2 flow was kept at 5 mL/min at 200 mA/cm^2 for ca. one hour for each run. Figure 3 presents the product distribution acquired at different RR.

Figure 3 presents similar selectivities for all RR, with CO at 70-80% while H_2 at 10-15% (while the remaining faradaic efficiency is believed to be formate, a lack of ability to test formate in the system means we do not know where the remaining current is going). Based on these results, the recycle loop had a negligible effect on Faradaic efficiency and conversion compared to the single-pass experiments. Besides, the increasing CO_2 inlet flow resulting from the recycle loop addition into the feeding rate seems not to significantly influence the conversion of CO_2, independent of the reaction temperature.

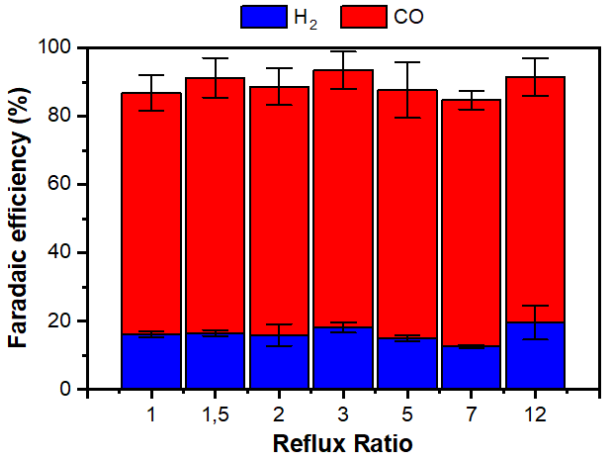

Figure 3: Effect of reflux ratio in the electrochemical conversion of CO_2 to CO. a) FE of main products at different reflux ratios. CO_2 inlet rate: 5 mL/min, current density: 200 mA/cm^2. Cathode: Ag membrane 1.2 μm Electrolyte 0.1M $KHCO_3$.

1.3.2 Effect of the recycle loop at high temperatures

The following section focuses on the influence of current density and the CO_2 inlet flow rate on CO_2 conversion using the recycle loop, with a constant R=3.0 and 60°C. The experiments consisted of catalytic screening at different current densities from 50 to 300 mA/cm^2 and an inlet flow rate (F_1) from 5 to 50 mL/min. Figure 4 depicts the CO_2 conversion to CO under various operating conditions. Compared to the previous results at room temperature, a CO_2 conversion into CO of up to 40% was achieved at 5 mL/min inlet flow. We can observe higher CO concentrations as a result of enhancing the CO_2 conversion kinetics at the active sites. In addition, the increased CO selectivity (visible in the gas chromatograph) at higher current densities could also be attributed to the improved gas diffusivity, CO_2 availability, and the weakened CO adsorption on the surface as a result of the recycle loop and high-temperature operations [10].

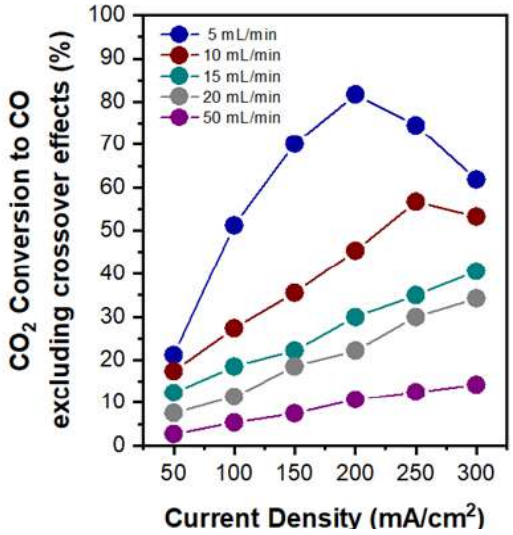

Figure 4: Effect of the current density and the feeding rate on CO_2 conversion to CO implementing the recycle loop.

Based on our experiments, we could see that rising the temperature could improve the diffusion limitations and improve the CO_2 mass transport, resulting in less pronounced hydrogen and higher CO production. Coupling the temperature with the recycle loop, we expect the reaction kinetics and diffusion coefficient to increase (which we can see in lower H_2 FE), lowering the activation overpotentials at operations below 200 mA/cm^2. However, when the current density exceeded this value high H_2 output occurred due to the CO_2 mass transport-limitation regime, which reduced CO selectivity.

1.3.3 eCO$_2$R PERFORMANCE AT THE LOW CO$_2$ INLET FLOW AND STABILITY TESTS

This section focuses on supporting the hypothesis proposed in the previous sections and achieving a 70% conversion of CO_2 at 200 mA/cm^2 and 60 °C mentioned in MS4.

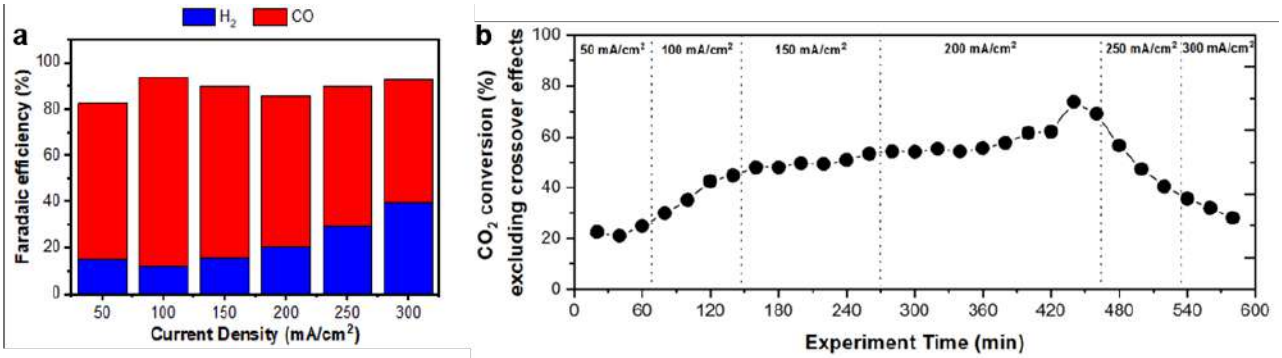

Figure 5: Effect of the current density in the electrochemical conversion of CO_2 to CO at 60 °C.

We first monitored the effect of the recycle loop and current density at 200 mA/cm^2. Using low CO_2 inlet rates (5 mL/min) with longer residence times, the CO_2 conversion can be improved. As revealed in Figure 5, the CO Faradaic efficiency and conversion were evidently enhanced as the current density increased from 50 to 200 mA/cm^2, as a result of the improved CO_2 diffusion due to a higher diffusion coefficient at higher temperatures, the increased local CO_2 concentration due to the improved mass transport and the reduced pH gradient from the bulk to the electrode/electrolyte interface.

Further measurements such as capacitance and capillarity pressure will provide more information on the beneficial effects of these conditions using the recycle line [12]. On the other hand, a similar trend presented in Figure 4 agrees with that in Figure 5, highlighting the limited eCO_2R (decreasing the CO production and favoring the HER) at current densities above 200 mA/cm^2 by merely increasing the temperature, where the CO_2 mass transport limitations and flooding are more visible in these experiments at current densities above 250 mA/cm^2.

Once all the optimal operating conditions were defined, a final experiment was conducted as a "stability test." A constant current density was applied, and the quantification of products was reported every ca.20 min for 8 hours. It is observed that in the first 2 hours, CO production gradually increased before reaching a maximum value of 86%, after which it remained stable for ~ 1h. A decay occurred afterward and then reached another plateau at ~70% and kept there for ca. six hours. Based on these results, the goal defined in Milestone 4 has been reached: an electrochemical CO_2 reduction conversion reaching 70% (excluding crossover) at a current density of 200 mA/cm^2 at 333 K.

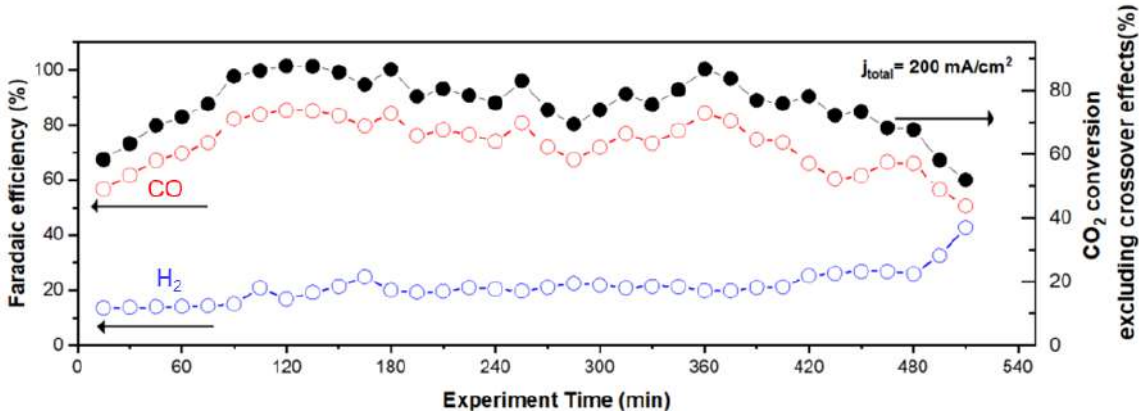

Figure 6: Long term experiment to study the FE of gas products and the CO_2 conversion to CO at 60 °C inlet rate: 5 mL/min at 200 mA/cm^2, cathode: commercial Ag membrane, membrane: MPIP 25 and electrolyte: 0.1 M $KHCO_3$

Although a higher FE of 86% was reached using the loop at 200 mA/cm^2 compared to single-pass experiments, it is still below the theoretical limit. There is a significant effect of carbonate formation on CO_2 consumption eCO_2R in neutral and alkaline media. Further studies focusing on a detailed carbon balance and crossover will provide more information regarding the above opinion and set up new approaches to the recycle loop line. The comparison of carbonate selectivity between theoretical values predicted from the Nernst-Planck equation, and experimental quantification from CO_2 crossover and the oxidation reactions at the anode will benefit the most. For measurements under higher current densities, carbonate-driven mechanisms will be favored from the high alkaline media, while the flooding resistance of the electrode will also be reduced. Therefore, modifications such as improving the hydrophobicity or gas-ion transport could help overcome these limitations in CO_2 conversion in single-pass experiments or implement the recycle line to improve the C_2 selectivity.

1.3.4 RESULTS AND DISCUSSION ON TEMPERATURE EFFECTS ON CO_2 REDUCTION

This section gives more attention to the temperature effect on eCO_2R performance by using the sputtered Cu, the benchmark catalyst for C_{2+} products. The CO_2 flow rate was set at 40 mL/min to prevent the influence of mass transport limitation. During the testing, we regulated the operating temperature from 30 to 80 °C and measured the product compositions.

1.3.5 Temperature Effect on Cell Voltage

The cell voltage changes at different temperatures were first exhibited in Figure 7. It shows a noticeable voltage drop with increasing temperatures at all current ranges. For example, a significant reduction of cell voltage from -3.4 V to -2.9 V is achieved to reach 200 mA/cm^2 when the operating temperature was elevated from 20 °C to 80 °C. We consider the main reason for the voltage decrease originates from the lower thermodynamic potential and activation overpotential for CO_2R and OER at higher temperatures [13]. Interestingly, a relatively more significant voltage drop was shown between 30 to 40 °C for current density > 200 mA/cm^2. We hypothesize that this phenomena is related to that at 30 °C there may be localized hot spots providing inconsistent humidification whereas at 40 °C and above the entire system should be at a more uniform temperature.

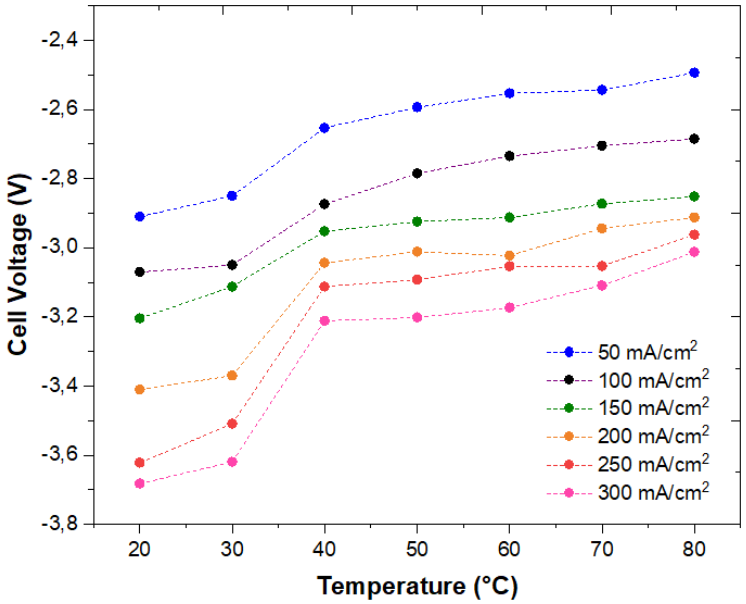

Figure 7: Cell voltage changes under different temperatures at current densities from 50 to 300 mA/cm^2. Inlet rate: 40 mL/min, cathode: sputtered Cu, membrane: MPIP 25 and electrolyte: 0.1 M $KHCO_3$.

1.3.6 Temperature Effect on eCO_2R Performance

To analyse the temperature effect on product distribution, the faradic efficiency (FE) of various gas and liquid products at different temperatures and current densities are exhibited in Figure 8. The FE loss (not equal to 100%) is due to the crossover of parts of liquid products to anode. They tend to be further oxidized at anode and thus not easy to sum to the total FE calculations.

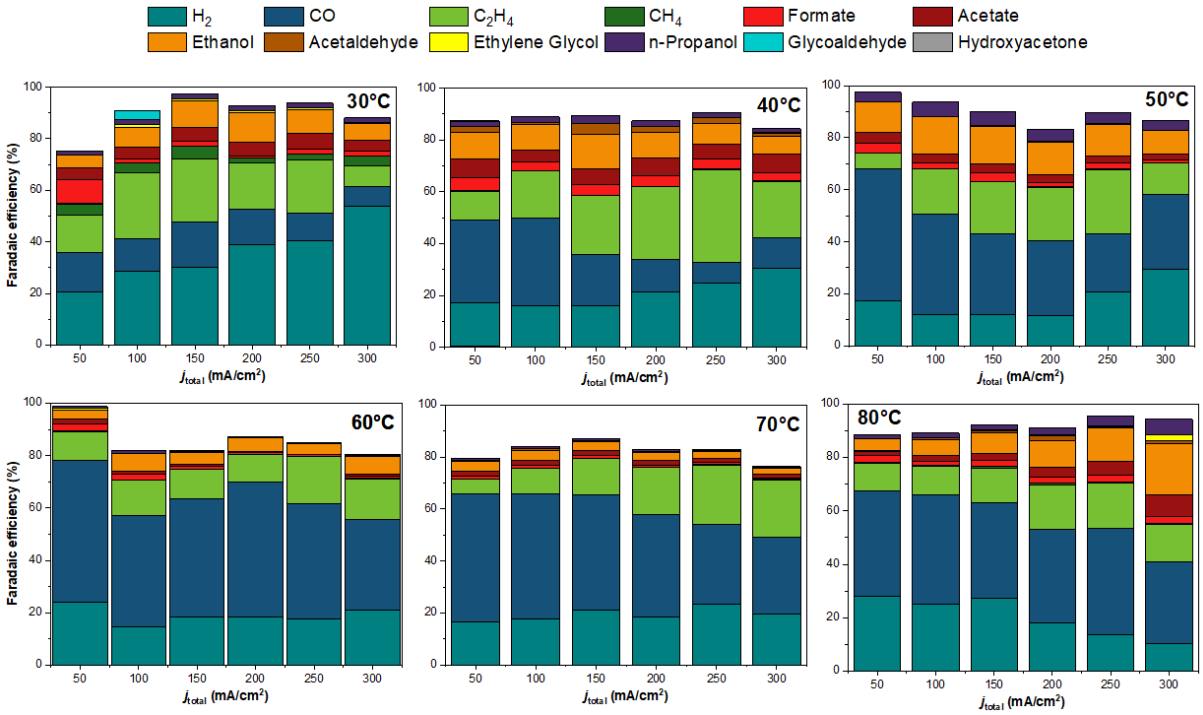

Figure 8: Product distributions of sputtered Cu catalyst for eCO2R under different temperatures at current densities from 50 to 300 mA/cm^2.

Figure 8 shows the FE of H_2 increases with current densities at 30 °C by previous studies [14]. However, after increasing the temperature up to 40 °C, the FE of H_2 decreases to ~20% and does not show the dependence on the current densities anymore. We summarized the FE ratios of CO_2R/HER at different current densities as a function of temperature in Figure 9a. It shows that the FE ratios for the curves of 50-200 mA/cm^2 have a peak at 50 °C while the FE ratios for the curves of 250-300 mA/cm^2 increase with the temperature and reach the top at 80 °C.

The highest FE ratio of CO_2R/HER (8.5) is achieved at operating condition of 300 mA/cm^2 and 80 °C. The above results indicate multiple factors, such as CO_2 solubility, humidity in the cell, activation overpotential, the conductivity of electrolytes, etc., which depend on the temperature, directly influence the FE of HER and CO_2R. For example, the decrease of CO_2 solubility and the increase of humidity in the cell at high temperature is favorable to HER. In contrast, the faster CO_2 mass transfer rate and smaller activation overpotential at high temperature is suitable for CO_2R. Therefore, when the mass transfer is still not the rate-determining step, *i.e.*, current densities < 200 mA/cm^2, the balance between either HER or CO_2R positive factors lead to the volcano-plots of CO_2R/HER ratios. On the other hand, at current densities > 250 mA/cm^2, the CO_2 mass transfer rate and activation overpotential would become the rate-limiting step for eCO2R. In this range, their improvements appear to be more significant than those of positive factors for HER and thus raise CO_2R/HER ratios with temperature.

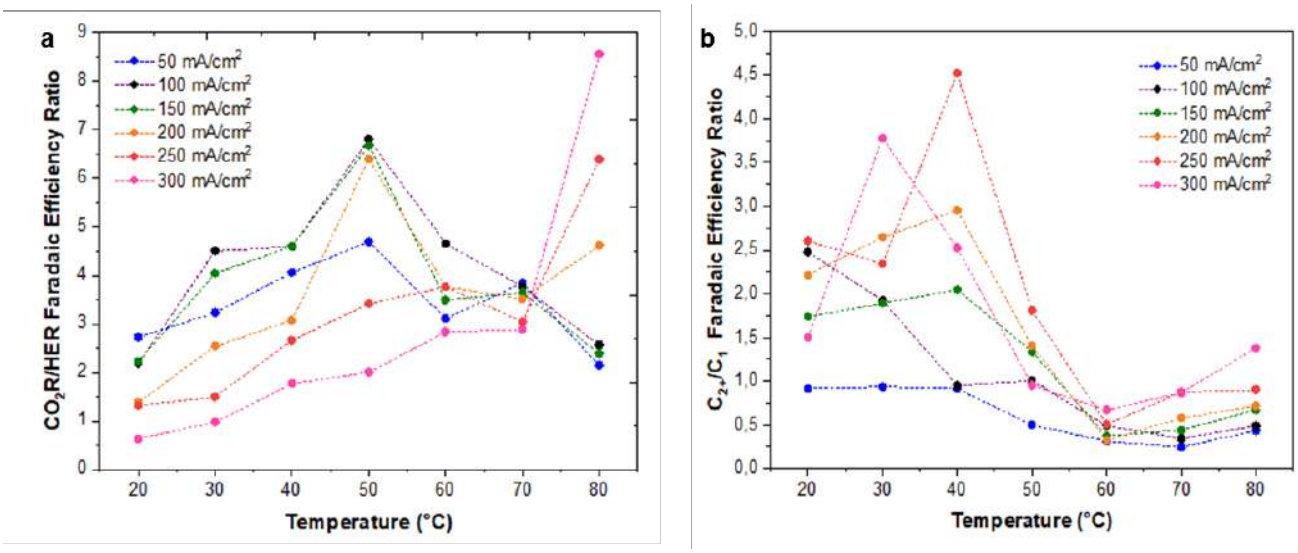

Figure 9: a) CO_2R/HER faradaic efficiency ratios and b) C_{2+}/C_1 faradaic efficiency ratios of sputtered Cu catalyst under different temperatures at current densities from 50 to 300 mA/cm^2.

Furthermore, temperature also affects the C_1 and C_{2+} product distribution of the sputtered Cu, which depends on more precise factors such as the potential reaction pathway variation and intermediates concentration change. In Figure 8, the highest FE of CO, CH_4, and C_2H_4 at 60 °C, 30 °C, and 40 °C, respectively, at almost all current ranges. Ethanol prefers to generate at 50 °C with an FE of ~15% at all current ranges. However, its FE also shows a trend with current densities at 80 °C and reaches 21% at 300 mA/cm^2. Figure 9b shows the FE ratios of C_{2+}/C_1 as a function of temperature. At current density < 100 mA/cm^2, the FE ratios of C_{2+}/C_1 decrease with temperature rise, indicating the desorption of *CO intermediate on the catalyst surface at higher temperatures.

The above experimental results have shown some brief temperature effects on cell voltage, FE of HER, and CO_2R, based on the sputtered Cu catalyst. In the next step, we will optimize the eCO_2R performance of the Cu catalyst by utilizing the recycle loop at different temperatures. More detailed experiments combined with synchronous characterization and theoretical calculation will be beneficial for clarifying the reaction mechanism of Cu catalyst at various temperatures.

1.4 References

.[1] Y. Zheng, A. Vasileff, X. Zhou, Y. Jiao, M. Jaroniec, and S. Z. Qiao, "Understanding the Roadmap for Electrochemical Reduction of CO2 to Multi-Carbon Oxygenates and Hydrocarbons on Copper-Based Catalysts," *J. Am. Chem. Soc.*, vol. 141, no. 19, pp. 7646–7659, 2019, doi: 10.1021/jacs.9b02124.

[2] S. Hernandez-Aldave and E. Andreoli, "Fundamentals of Gas Diffusion Electrodes and Electrolysers for Carbon Dioxide Utilisation: Challenges and Opportunities," *Catalysts*, vol. 10, no. 6, p. 713, 2020, doi: 10.3390/catal10060713.

[3] U. O. Nwabara, E. R. Cofell, S. Verma, E. Negro, and P. J. A. Kenis, "Durable Cathodes and Electrolyzers for the Efficient Aqueous Electrochemical Reduction of CO2," *ChemSusChem*, vol. 13, no. 5, pp. 855–875, 2020, doi: 10.1002/cssc.201902933.

[4] S. Ma, M. Sadakiyo, R. Luo, M. Heima, M. Yamauchi, and P. J. A. Kenis, "One-step electrosynthesis of ethylene and ethanol from CO2 in an alkaline electrolyzer," *J. Power Sources*, vol. 301, pp. 219–228, Jan. 2016, doi: 10.1016/J.JPOWSOUR.2015.09.124.

[5] C. M. Gabardo *et al.*, "Continuous Carbon Dioxide Electroreduction to Concentrated Multi-carbon Products Using a Membrane Electrode Assembly," *Joule*, vol. 3, no. 11, pp. 2777–2791, 2019, doi: 10.1016/j.joule.2019.07.021.

[6] C. M. Gabardo *et al.*, "Combined high alkalinity and pressurization enable efficient CO2 electroreduction to CO," *Energy Environ. Sci.*, vol. 11, no. 9, pp. 2531–2539, 2018, doi: 10.1039/c8ee01684d.

[7] E. J. Dufek, T. E. Lister, and M. E. McIlwain, "Influence of electrolytes and membranes on cell operation for Syn-Gas Production," *Electrochem. Solid-State Lett.*, vol. 15, no. 4, pp. 48–51, 2012, doi: 10.1149/2.010204esl.

[8] M. Jouny, W. Luc, and F. Jiao, "General Techno-Economic Analysis of CO2 Electrolysis Systems," *Ind. Eng. Chem. Res.*, vol. 57, no. 6, pp. 2165–2177, 2018, doi: 10.1021/acs.iecr.7b03514.

[9] C. T. Dinh, Y. C. Li, and E. H. Sargent, "Boosting the Single-Pass Conversion for Renewable Chemical Electrosynthesis," *Joule*, vol. 3, no. 1, pp. 13–15, 2019, doi: 10.1016/j.joule.2018.10.021.

[10] E. Jeng and F. Jiao, " Investigation of CO 2 single-pass conversion in a flow electrolyzer ," *React. Chem. Eng.*, vol. 5, no. 9, pp. 1768–1775, 2020, doi: 10.1039/d0re00261e.

[11] G. O. Larrazábal *et al.*, "Analysis of Mass Flows and Membrane Cross-over in CO2 Reduction at High Current Densities in an MEA-Type Electrolyzer," *ACS Appl. Mater. Interfaces*, vol. 11, no. 44, pp. 41281–41288, 2019, doi: 10.1021/acsami.9b13081.

[12] M. E. Leonard, L. E. Clarke, A. Forner-Cuenca, S. M. Brown, and F. R. Brushett, "Investigating Electrode Flooding in a Flowing Electrolyte, Gas-Fed Carbon Dioxide Electrolyzer," *ChemSusChem*, vol. 13, no. 2, pp. 400–411, 2020, doi: 10.1002/cssc.201902547.

[13] B. Endrődi, G. Bencsik, F. Darvas, R. Jones, K. Rajeshwar, and C. Janáky, "Continuous-flow electroreduction of carbon dioxide," *Prog. Energy Combust. Sci.*, vol. 62, pp. 133–154, 2017, doi: 10.1016/j.pecs.2017.05.005.

[14] M. Ma, E. L. Clark, K. T. Therkildsen, S. Dalsgaard, I. Chorkendorff, and B. Seger, " Insights into the carbon balance for CO 2 electroreduction on Cu using gas diffusion electrode reactor designs ," *Energy Environ. Sci.*, vol. 13, no. 3, pp. 977–985, 2020, doi: 10.1039/d0ee00047g.

[15] A. Pătru, T. Binninger, B. Pribyl, and T. J. Schmidt, "Design Principles of Bipolar Electrochemical Co-Electrolysis Cells for Efficient Reduction of Carbon Dioxide from Gas Phase at Low Temperature," *J. Electrochem. Soc.*, vol. 166, no. 2, pp. F34–F43, 2019, doi: 10.1149/2.1221816jes.

[16] T. Haas, R. Krause, R. Weber, M. Demler, and G. Schmid, "Technical photosynthesis involving CO2 electrolysis and fermentation," *Nat. Catal.*, vol. 1, no. 1, pp. 32–39, 2018, doi: 10.1038/s41929-017-0005-1.

[17] Y. C. Li *et al.*, "Electrolysis of CO2 to Syngas in Bipolar Membrane-Based Electrochemical Cells," *ACS Energy Lett.*, vol. 1, no. 6, pp. 1149–1153, 2016, doi: 10.1021/acsenergylett.6b00475.

[18] D. A. Salvatore *et al.*, "Electrolysis of Gaseous CO2 to CO in a Flow Cell with a Bipolar Membrane," *ACS Energy Lett.*, vol. 3, no. 1, pp. 149–154, 2018, doi: 10.1021/acsenergylett.7b01017.

[19] S. Verma *et al.*, "Insights into the Low Overpotential Electroreduction of CO2 to CO on a Supported Gold Catalyst in an Alkaline Flow Electrolyzer," *ACS Energy Lett.*, vol. 3, no. 1, pp. 193–198, 2018, doi: 10.1021/acsenergylett.7b01096.

[20] Z. Liu *et al.*, "Electrochemical generation of syngas from water and carbon dioxide at industrially important rates," *J. CO2 Util.*, vol. 15, pp. 50–56, 2016, doi: 10.1016/j.jcou.2016.04.011.

[21] R. B. Kutz, Q. Chen, H. Yang, S. D. Sajjad, Z. Liu, and I. R. Masel, "Sustainion Imidazolium-Functionalized Polymers for Carbon Dioxide Electrolysis," *Energy Technol.*, vol. 5, no. 6, pp. 929–936, 2017, doi: 10.1002/ente.201600636.

[22] J. He, Y. Li, A. Huang, Q. Liu, and C. Li, *Electrolyzer and Catalysts Design from Carbon Dioxide to Carbon Monoxide Electrochemical Reduction*, no. 0123456789. Springer Singapore, 2021.

[23] X. Liu, J. Xiao, H. Peng, X. Hong, K. Chan, and J. K. Nørskov, "Understanding trends in electrochemical carbon dioxide reduction rates," *Nat. Commun.*, vol. 8, no. May, pp. 1–7, 2017, doi: 10.1038/ncomms15438.

[24] S. Nitopi *et al.*, "Progress and Perspectives of Electrochemical CO2 Reduction on Copper in Aqueous Electrolyte," *Chem. Rev.*, vol. 119, no. 12, pp. 7610–7672, 2019, doi: 10.1021/acs.chemrev.8b00705.

[25] T. Möller, T. N. Thanh, X. Wang, W. Ju, Z. Jovanov, P. Strasser, Energy Environ. Sci., 2021,14, 5995-6006.

[26] M. J. Moran, H. N. Shapiro, D. D. Boettner and M. B. Bailey, Fundamentals of engineering thermodynamics, John Wiley & Sons, 2010